Computer Methods and Programs in Biomedicine 221 (2022) 106859

Contents lists available at ScienceDirect

Computer Methods and Programs in Biomedicine

journal homepage: www.elsevier.com/locate/cmpb

Classification of code-modulated visual evoked potentials using adaptive modified covariance beamformer and EEG signals

Asghar Zarei, Babak Mohammadzadeh Asl*

Department of Biomedical Engineering, Tarbiat Modares University, Tehran, Iran

ARTICLE INFO

Article history:
Received 27 September 2021
Revised 17 April 2022
Accepted 5 May 2022

Keywords:
BCI
c-VEP
Adaptive and parameter-free covariance matrix estimators
Spatiotemporal beamforming
EEG ignal

ABSTRACT

Objective: In general, brain computer interface (BCI) studies based on code-modulated Visual Evoked Potentials (c-VEP) use m-sequences to decode EEG responses to visual stimuli. BCI systems based on the c-VEP paradigm can simultaneously present a large number of commands, which results in a significantly high information transfer rate (ITR). Spatiotemporal beamforming (STB) is one of the commonly used approaches in c-VEP-based BCI systems. Approach: In the current work, a novel STB-based technique is proposed to detect the gazed targets. The proposed method improves the performance of conventional STB-based techniques by providing a robust estimation of the covariance matrix in short stimulation times. Different user parameter-free methods, including the convex combination (CC), the general linear combination (GLC), and the modified versions of these techniques, are used to estimate a reliable and robust covariance matrix when a small number of repetitions are available. Main results: The stimulus presentation rate of 120 *Hz* is used to assess the performance of the proposed structures. Our proposed methods improved the classification accuracy by an average of 20% compared to the conventional STB method at the shortest stimulation time. The proposed method achieves an average ITR of 157.07 bits/min by using only two repetitions of the m-sequences. Significance: The results show that our proposed methods perform significantly better than the conventional STB technique in all stimulation times.

1. Introduction

Code modulated visual evoked potentials (c-VEPs) are created as a result of visual stimuli modulated by a binary code (with zero and one values). This code is defined based on the low and high intensities of the stimulus, and it is unique for each of the c-VEP targets. In other words, each of the targets is coded using a unique lagged version of the defined pseudorandom code. The m-sequence is one of the commonly pseudorandom sequences in c-VEP-based brain-computer interfaces (BCIs). An m-sequence is roughly orthogonal to its time-delayed versions and it has desirable statistical properties [1]. Therefore, the m-sequence is usually selected to build c-VEP-based BCI systems. In recent years, however, some alternative methods have been proposed instead of m-sequence, such as [2] and [3].

The flickering speed is one of the most important parameters that affect the classification accuracy. Won and colleagues reported that the stimulus can cause mental fatigue, thereby reducing the applicability of BCI systems [4]. Furthermore, patterns with a low flickering speed can intensify photosensitivity-based epileptic seizures [4]. So far, several studies have investigated the effect of using different stimulus presentation frequencies in c-VEP-based BCIs, e.g., [5], [6], and [7].

Because of the high information transfer rate (ITR) property of cVEP-based BCIs, these systems have expanded significantly in recent years. It should be noted that c-VEPs are brain responses that can be decoded using electroencephalography (EEG) over the occipital lobe. So far, various methods such as template matching ([8] and [1]), canonical correlation analysis (CCA) and its extended versions ([5,8–10]), and spatiotemporal beamforming ([2] and [11]), have been developed to decode c-VEP responses using EEG signals. These methods have shown great potentials for different BCI applications, and they can be applied to other physiological signals, such as intracranial EEG and electrocorticography (ECoG), in an online manner.

Over the last few years, different extended versions of beamforming algorithms (i.e., the spatial, temporal, and spatiotemporal forms) have been employed in EEG-based BCI systems [12–15]. In [13], the authors extended the linearly constrained minimum variance (LCMV) beamformer as a flexible spatiotemporal filter to estimate the amplitude of event related potential (ERP) components in the sensor space. In another study, the authors developed a

* Corresponding author.
E-mail address: babakmasl@modares.ac.ir (B. Mohammadzadeh Asl).

https://doi.org/10.1016/j.cmpb.2022.106859
0169-2607/

novel spatial form of the beamforming algorithm for the localization of cortical activity from single-trial neuromagnetic recordings [16]. Wittevrongel and Van Hulle applied the spatiotemporal extension of the LCMV beamformer to classify P300 responses. They have shown that the beamformer has almost the same classification performance as the SVM (state-of-the-art classifier); however its training speed is many times faster than the SVM [17]. Also, Sabeti *et al*. developed a new form of the LCMV beamformer to localize brain sources of P300 potentials [18].

The beamformer captures the component of interest using two important parameters, i.e., the pre-defined templates (activation patterns) and the estimation of the data covariance matrix [13]. One of the main problems in all the state-of-the-art proposed methods is that their performance reduces when using short segment lengths. In [2] and [11], the authors have shown that beamformer-based techniques outperform other state-of-the-art methods in short stimulation times. Robust estimation of the covariance matrix is needed to develop a robust beamforming-based technique. It is noteworthy that when a short segment length is used, an accurate and robust estimation of the covariance matrix is not provided. On the other hand, using short segment lengths can increase the ITR and the speed of the BCI system and reduce the mental fatigue caused by stimulation representation. Traditionally, the diagonal loading (DL) method is usually applied to provide a more robust data covariance matrix [19,20]. The main deficiency of the DL technique is that the proper DL factor is not determined automatically, which is one of the main challenges. To deal with this problem, different forms of shrinkage methods, such as general linear combination (GLC) and convex combination (CC), have been presented in signal processing applications [21,22]. These are user parameter-free methods in which all the parameters are automatically and adaptively determined using the mean-square error (MSE) concept.

To address the above-mentioned problem, i.e., performance reduction when using short segment length EEG signals, we assess the performance of different beamforming algorithms for c-VEP target classification. In this study, we investigate different forms of user parameter-free adaptive methods (i.e., the GLC, CC, and their extended forms) to provide a robust estimation of the covariance matrix. Then, we propose a novel spatiotemporal beamformer for c-VEP target identification using robust and adaptive covariance matrix estimators. To the best of our knowledge, this is the first study to investigate the effectiveness of shrinkage-based adaptive covariance matrix estimators in the application of c-VEP-based BCI systems.

The rest of the article is organized as follows. Section 2 describes the database along with the proposed methods. The results of the proposed methods and discussions are presented in Sections 3 and 4, respectively. Finally, Section 5 concludes the paper.

Notations: Throughout the rest of this paper, we denote vectors and matrices by boldface lowercase and uppercase letters, respectively. The subscript $E\{.\}$ denotes the mathematical expectation operator, $trace(.)$ denotes the trace operator, $\|.\|$ is the Frobenius norm for a matrix or the Euclidean norm for a vector, $(.)^*$ denotes the conjugate transpose, and $(.)^T$ denotes the transpose. Finally, $\mathbf{I}$ denotes the identity matrix.

2. Materials and methods

2.1. The proposed framework

In the current study, a novel solution for c-VEP target detection is proposed using parameter-free adaptive covariance matrix estimation techniques and short times EEG signals. As described in the previous section, only a poor estimation of the covariance matrix is provided in short stimulation times. Therefore, most beamforming-based methods lose their optimum performance. To tackle this problem, we use different forms of knowledge-aided adaptive covariance matrix estimation techniques. These parameter-free methods include GLC, CC, and their extended versions, in which a robust estimation of the covariance matrix is provided. Thus, in this study, we combine the above-mentioned adaptive methods with the spatiotemporal form of the LCMV beamformer to develop a robust spatiotemporal beamformer. The flowchart of the proposed c-VEP target detection framework is demonstrated in Fig. 1. According to this figure, in the training phase, a unique beamformer and template (activation pattern) are calculated for each target. In the test phase, each of the designed beamformers is applied separately to the input segment, and the output label is specified after applying the threshold to the beamformers' outputs.

2.2. EEG Dataset

This dataset contains 17 EEG recordings, recorded using a Neuroscan SynampsRT device with 32 active Ag/AgCl electrodes from 17 subjects. The age of the subjects varies from 18 to 30 years. An interface with 32 circular white targets was used [23]. The targets were presented at a stimulation rate of 120 *Hz*, and they were encoded using a binary m-sequence with a length of 63 *bits* and its lagged versions. The stimulus duration of a 63 *bits* m-sequence is $63/120 = 0.525$ second. In each trial, at first, a cue was shown to the subjects. Then, by displaying this cue, subjects had to focus on all the targets simultaneously stimulated by their specific m-sequence. Each target was presented five times. Therefore, 160 trials were provided. The sampling rate of each recording is 1000 *Hz*. All the EEG signals were filtered between 4 and 31 *Hz*. Then, all the filtered EEG signals were cut into 5.25-second segments and downsampled to 200 *Hz*. Finally, each segment was labeled based on the cued target. All the necessary information on this dataset can be found in [23].

2.3. Beamforming

As noted in the previous sections, one of the main challenges present in all existing methods is the reduction in the optimal performance of the methods when using short stimulation times. In other words, reducing the length of the segment leads to a reduction in the classification accuracy of the existing approaches. The beamformer is a filter that performs better than the state-of-the-art techniques in the classification of c-VEP responses using EEG signals with short segments (short stimulation times) [23]. However, the performance of the beamformer-based techniques is highly dependent on the estimation of the data covariance matrix. When using short segment lengths, the performance of the conventional STB-based beamformers reduces because of the poor estimation of the covariance matrix. In practice, different solutions, such as DL [19,20], GLC, CC [21,22], and their extended forms [24], have been presented in various fields of study, to provide a robust estimation of the covariance matrix. In this study, we design a novel adaptive robust beamformer for the classification of c-VEP responses using modified covariance matrix estimation methods.

The beamformer is a filter made using two basic parameters, i.e., the activation pattern and the data covariance matrix. Each target elicits a unique c-VEP response based on its specific m-sequence. As a result, a unique activation pattern should be calculated for each of the targets. In this study, 32 activation patterns (here we have 32 targets) are calculated. Hence, we construct 32 beamformers using the training data set. Therefore, for each subject, all the developed beamformers were target-specific, and we analyzed the classification performance in a subject-dependent manner. The performance of the beamformer-based techniques

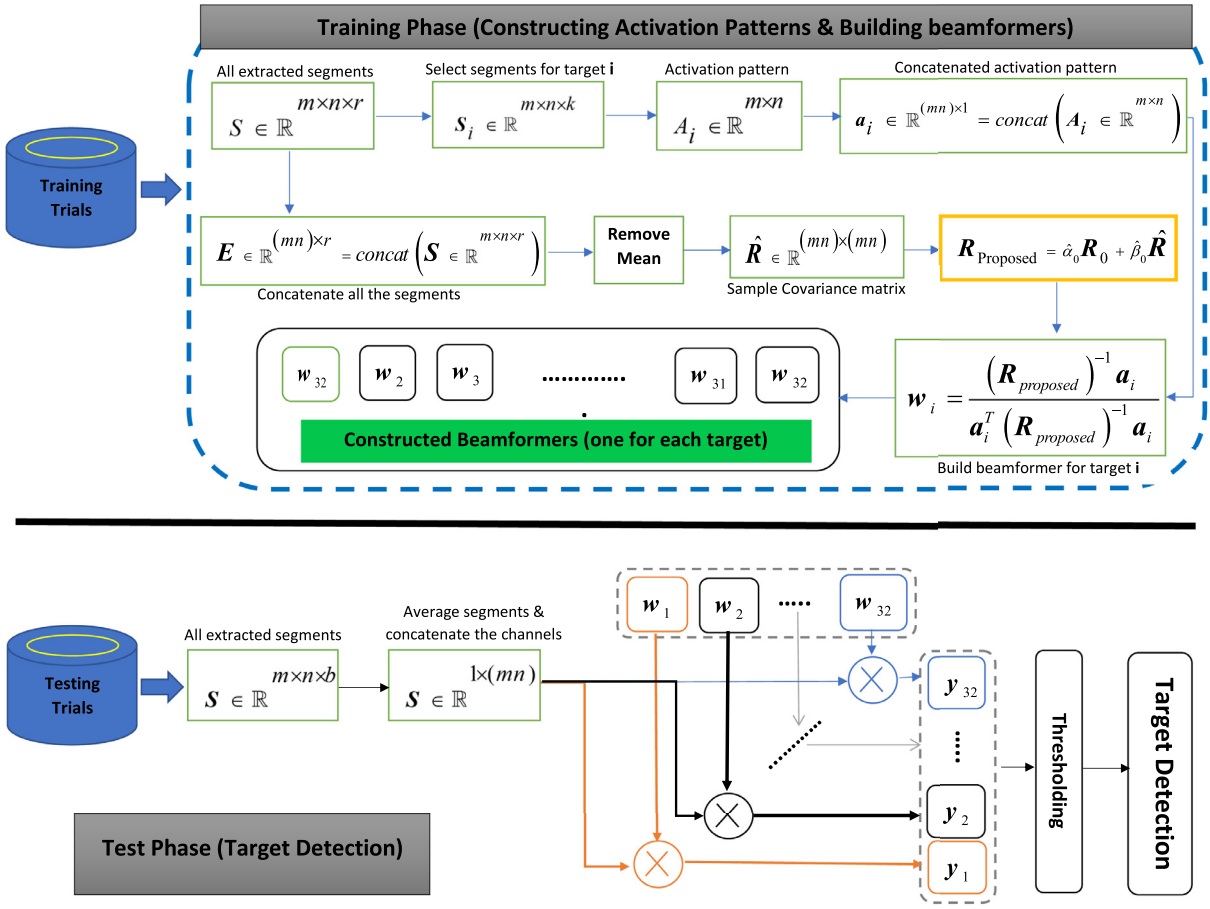

Fig. 1. The block diagram of the proposed method for building beamformers, calculating activation patterns, and cVEP target detection.

highly depends on the activation pattern (**A**) and the data covariance matrix (**R**). In this study, both are estimated from the EEG data.

2.3.1. The activation pattern

Let $\mathbf{D}_{train} \in \mathbb{R}^{m\times n\times l}$ be the training dataset. Here, m, n, and l are the number of the electrodes, samples, and epochs, respectively. Assume that $\mathbf{S} \in \mathbb{R}^{m\times n\times r}$ is the total number of segments extracted from the training dataset. Here, r is the number of extracted segments. Moreover, suppose that $\mathbf{S_i} \in \mathbb{R}^{m\times n\times k}$ indicates the extracted segments in response to the cued target. For these parameters, n represents the number of samples and $i \in [1, \ldots, 32]$ represents the number of selectable targets. It should be noted that the temporal, spatial, and spatiotemporal activation patterns must be calculated for the development of temporal, spatial, and spatiotemporal beamformers, respectively. In this study, the spatiotemporal activation pattern $\mathbf{A_i} \in \mathbb{R}^{m\times n}$ for target i is calculated by averaging all the segments extracted from $\mathbf{S_i}$.

2.3.2. The spatiotemporal beamformer (STB)

As mentioned in the previous section, building a beamformer involves calculating the activation pattern and estimating the data covariance matrix. Each target elicits a unique c-VEP response. Therefore, in the training phase, a unique beamformer is designed for each target using the training dataset. The pseudo-code used to build the STB parameters is presented in Algorithm 1. As shown in this algorithm, the STB method gives all the segments extracted from target i in its input and returns the designed beamformer ($\mathbf{w}_i$) in the output. In Algorithm 1 the subscript $concat(.)$ denotes the concatenate operator. For example, for computing $\mathbf{a}_i^T$, this operator can be mathematically applied to $\mathbf{A}_i$ as follows:

$$\mathbf{a}_i^T \in \mathbb{R}^{1\times(mn)} = \{b_{1,1}, \ldots, b_{1,m}, \ldots, b_{n,1}, \ldots, b_{n,m}\} = concat\left\{\mathbf{A}_i = \begin{bmatrix} b_{1,1} & \cdots & b_{1,m} \\ \vdots & \ddots & \vdots \\ b_{n,1} & \cdots & b_{n,m} \end{bmatrix}\right\} \quad (1)$$

2.3.3. Covariance matrix

In practice, the true data covariance matrix (**R**) is not available. Therefore, as an alternative, the sample covariance matrix ($\hat{\mathbf{R}}$) is calculated as follows:

$$\hat{\mathbf{R}} = \frac{1}{M}\sum_{i=1}^{M}\left(\mathbf{X}(i)\mathbf{X}(i)^T\right) \quad (2)$$

where $\mathbf{X}$ and M denote the sample data matrix and number of samples, respectively. In [25], the authors have reported that when the number of time samples is small, the sample covariance matrix ($\hat{\mathbf{R}}$) is sensitive to noise; hence, it is not the optimum choice. Moreover, one of the main challenges in STB-based methods is that their performance reduces when the stimulation time is low. To deal with this problem, user parameter-free robust adaptive covariance matrix estimators are presented in the next sections.

2.3.4. The diagonal loading method

To improve the robustness of the STB method, the DL method [20] has been proposed, in which the weight vector is calculated

Algorithm 1 The STB method.

Input: All the segments extracted for target i : $\mathbf{S_i} \in \mathbb{R}^{m\times n\times k}$

Output: Constructed spatiotemporal beamformer for target i : $\mathbf{w_i} \in \mathbb{R}^{(mn)\times 1}$

N = 32 is the number of selectable targets,
for $i = 1$ to N **do**
  Select segments from target i = $\mathbf{S}_i \in \mathbb{R}^{m\times n\times k}$
  $\mathbf{A_i} \in \mathbb{R}^{m\times n} = \frac{1}{k}\sum_{j=1}^{k}\mathbf{S}_i(m,n,j)$,
  Calculate $\mathbf{a}_i^T \in \mathbb{R}^{1\times(mn)} = concat(\mathbf{A_i} \in \mathbb{R}^{m\times n})$
  Calculate $\mathbf{E} \in \mathbb{R}^{(mn)\times r} = concat(S \in \mathbb{R}^{m\times n\times r})$,
  Remove the mean of $\mathbf{E}$: $\mathbf{E} = \mathbf{E} - mean(\mathbf{E})$
  Calculate $\hat{\mathbf{R}} \in \mathbb{R}^{(mn)\times(mn)} = \frac{1}{r-1}\mathbf{E}\mathbf{E}^T$,
  Consider the constraint $\mathbf{a}_i^T\mathbf{w}_i = 1$
  Use the Lagrange multipliers to build the spatiotemporal beamformer as follows:$\mathbf{w}_i = \frac{\hat{\mathbf{R}}^{-1}\mathbf{a}_i}{\mathbf{a}_i^T\hat{\mathbf{R}}^{-1}\mathbf{a}_i}$
end for
return 32 beamformers (one for each target)

as follows:

$$\mathbf{w}_{DL} = \frac{(\hat{\mathbf{R}} + \lambda\mathbf{I})^{-1}\mathbf{a}}{\mathbf{a}^T(\hat{\mathbf{R}} + \lambda\mathbf{I})^{-1}\mathbf{a}} \tag{3}$$

where λ is the DL factor, which is usually chosen manually (the main drawback of the DL approach). However, the determination of the proper DL factor has always been a challenge.

2.3.5. Shrinkage based robust parameter-free methods

Shrinkage methods, including general linear combination (GLC), convex combination (CC), and their extended versions, are other solutions for increasing the robustness of the STB method. In these techniques, a more robust and confident estimation of the covariance matrix is provided using a linear combination between the identity matrix ($\mathbf{I}$) and the sample covariance matrix ($\hat{\mathbf{R}}$). In contrast to the DL method, shrinkage parameters are obtained automatically and adaptively. As far as we know, the performance of GLC, CC, and their extended versions in c-VEP-based BCI systems has not yet been analyzed.

In this study, different shrinkage-based robust and adaptive user parameter-free techniques, including GLC, CC, and their modified versions, are used to address the small sample size (or short stimulation time) problem, in the sample covariance matrix estimation ($\hat{\mathbf{R}}$). Therefore, the $\hat{\mathbf{R}}$ is replaced by a robust and enhanced estimation of the sample covariance matrix provided using the shrinkage-based methods. The mean square error (MSE) concept is utilized to obtain a linear combination between $\hat{\mathbf{R}}$ and $\mathbf{R}_0$ matrices. In the CC technique, an enhanced estimate of the covariance matrix is presented as follows:

$$\tilde{\mathbf{R}}_{\mathbf{CC}} = \alpha\mathbf{R}_0 + (1-\alpha)\hat{\mathbf{R}}, \tag{4}$$

where α and $\mathbf{R}_0$ are the shrinkage intensity and a non-random matrix (usually the identity matrix $\mathbf{I}$), respectively. Furthermore, a more general form, i.e., the GLC method, can be formulated as follows:

$$\tilde{\mathbf{R}}_{\mathbf{GLC}} = \alpha\mathbf{R}_0 + \beta\hat{\mathbf{R}}. \tag{5}$$

The MSE of $\tilde{\mathbf{R}}$, i.e, $MSE(\tilde{\mathbf{R}}) = E\left\{\left\|\tilde{\mathbf{R}} - \mathbf{R}\right\|^2\right\}$, is used to choose the shrinkage parameters (α and β). Note that the enhanced estimate of $\mathbf{R}$ (i.e., $\tilde{\mathbf{R}}$) should satisfy $\tilde{\mathbf{R}} \geq 0$. To guarantee this fact, the constraints $\alpha \in [0,1]$ for the CC method and $\beta \geq 0, \alpha \geq 0$ for the GLC technique can be considered.

The MSE minimization for GLC method is defined as follows:

$$\begin{aligned}\alpha,\beta &= \arg\min_{\alpha,\beta} \mathrm{MSE} = E\left\{\left\|\tilde{\mathbf{R}} - \mathbf{R}\right\|_F^2\right\}\\ &= \|\alpha\mathbf{R_0} - (1-\beta)\mathbf{R}\|^2 + \beta^2 E\left\{\left\|\hat{\mathbf{R}} - \mathbf{R}\right\|^2\right\}\\ &= \alpha^2\|\mathbf{R_0}\|^2 - 2\alpha(1-\beta)trace(\mathbf{R}_0^*\mathbf{R}) + (1-\beta)^2\|\mathbf{R}\|^2\\ &\quad + \beta^2 E\left\{\left\|\hat{\mathbf{R}} - \mathbf{R}\right\|^2\right\}.\end{aligned}$$

$$s.t.\ \tilde{\mathbf{R}}_{\mathbf{GLC}} = \alpha\mathbf{R}_0 + \beta\hat{\mathbf{R}}, \tag{6}$$

where $\mathbf{R}_0^*$ is the conjugate transpose form of $\mathbf{R}_0$. As a result, the unconstrained optimal values for α_0 and β_0 can be calculated as follows:

$$\beta_0 = \frac{\gamma}{\gamma+\rho}, \tag{7}$$

$$\alpha_0 = \nu(1-\beta_0) = \nu\frac{\rho}{\gamma+\rho}, \tag{8}$$

where $\gamma = \frac{\|\mathbf{R}\|^2\|\mathbf{R}_0\|^2 - trace^2[\mathbf{R}_0^*\mathbf{R}]}{\|\mathbf{R}_0\|^2}$, $\rho = E\left\{\left\|\hat{\mathbf{R}} - \mathbf{R}\right\|^2\right\}$, and $\nu = \frac{trace[\mathbf{R}_0^*\mathbf{R}]}{\|\mathbf{R}_0\|^2}$. It should be noted that here $\beta_0 \in [0,1]$ and $\alpha_0 \geq 0$. In practice, the true covariance matrix ($\mathbf{R}$) is not available. Therefore, the true value of ρ can not be calculated. Instead, for a given data, the value of $\hat{\rho}$ can be estimated as follows:

$$\hat{\rho} = \frac{1}{M^2}\sum_{j=1}^{M}\|\mathbf{X}(j)\|^4 - \frac{1}{M}\left\|\hat{\mathbf{R}}\right\|^2. \tag{9}$$

where M is the number of samples, $\mathbf{X}(.)$ is the data with zero mean, and $\hat{\mathbf{R}}$ represents the sample covariance matrix. Also, we can estimate the values of ν and γ as follows:

$$\hat{\nu} = \frac{trace(\mathbf{R}_0^*\hat{\mathbf{R}})}{\|\mathbf{R}_0\|^2}, \tag{10}$$

$$\hat{\gamma} = \frac{\left\|\hat{\mathbf{R}}\right\|^2\|\mathbf{R}_0\|^2 - trace^2\left[\mathbf{R}_0^*\hat{\mathbf{R}}\right]}{\|\mathbf{R}_0\|^2}. \tag{11}$$

Consequently, an alternative to $\gamma + \rho = E\left\{\left\|\hat{\mathbf{R}} - \nu\mathbf{R}_0\right\|^2\right\}$ can be estimated as follows:

$$\hat{\gamma} + \hat{\rho} = \left\|\hat{\mathbf{R}} - \hat{\nu}\mathbf{R}_0\right\|^2. \tag{12}$$

Then, the alternative estimations of β_0 and α_0 can be expressed as follows:

$$\hat{\beta}_0 = \frac{\hat{\gamma}}{\hat{\gamma}+\hat{\rho}}, \tag{13}$$

$$\hat{\alpha}_0 = \hat{\nu}\left(1-\hat{\beta}_0\right) = \hat{\nu}\frac{\hat{\rho}}{\hat{\gamma}+\hat{\rho}}. \tag{14}$$

Furthermore, the non-negative alternative estimates of β_0 and α_0 can be calculated as follows:

$$\hat{\alpha}_0 = \min\left[\hat{\nu}\frac{\hat{\rho}}{\left\|\hat{\mathbf{R}} - \hat{\nu}\mathbf{R}_0\right\|^2}, \hat{\nu}\right], \tag{15}$$

$$\hat{\beta}_0 = 1 - \frac{\hat{\alpha}_0}{\hat{\nu}}. \tag{16}$$

In Equation (15), the minimum value between two expressions $\hat{\nu}$ and $\hat{\nu}\frac{\hat{\rho}}{\left\|\hat{\mathbf{R}}-\hat{\nu}\mathbf{R}_0\right\|^2}$ is chosen. For the CC method, we set $\hat{\nu} = 1$ to estimate the shrinkage parameter ($\hat{\alpha}_0$) using the Equation (15). Finally, the enhanced estimation of the covariance matrix for GLC technique can be formulated as follows:

$$\tilde{\mathbf{R}}_{GLC} = \hat{\alpha}_0\mathbf{R}_0 + \hat{\beta}_0\hat{\mathbf{R}}, \tag{17}$$

and for CC method we can use the following relation:

$$\tilde{\mathbf{R}}_{\mathbf{CC}} = \hat{\alpha}_0\mathbf{R}_0 + (1-\hat{\alpha}_0)\hat{\mathbf{R}}. \tag{18}$$

The pseudo-code for calculating the shrinkage parameters, $\tilde{\mathbf{R}}_{GLC}$, and $\mathbf{w}_{GLC}$ is presented in Algorithm 2. In all previous equations $\mathbf{R}_0$ is considered equal to the identity matrix ($\mathbf{I}$).

2.4. Different proposed structures

It is worth noting that when short-length segments are used, an accurate estimate of the covariance matrix is not provided in conventional methods. Moreover, when the number of independent time samples is less than the number of electrodes (M), the sample covariance matrix loses its full rank property. As a result, the sample covariance matrix becomes singular and cannot be inverted. Mathematically, it is proven that at least 3M to 4M statistically-independent observations are needed for the accurate estimation of the data covariance matrix [26]. Hence, even if the number of samples becomes more than M, an accurate estimation of the covariance matrix is not possible. To overcome this problem, in practice some noise ($\mathbf{R_0}$) is added to the sample covariance matrix ($\hat{\mathbf{R}}$). In addition to the proposed adaptive covariance matrix estimators, i.e., the GLC and CC techniques, we use different estimations of $\mathbf{R_0}$ instead of the identity matrix ($\mathbf{I}$) in Equations (17) and (18). In other words, instead of $\mathbf{R_0}$ matrix, different structures are used to obtain robust covariance matrix estimators. Selecting a suitable structure for $\mathbf{R_0}$ plays an important role in the performance of the covariance matrix estimator. One of the commonly used structures is $\mathbf{R_0} = \mathbf{I}$ (here $\mathbf{I}$ is the identity matrix). This structure ($\mathbf{R_0} = \mathbf{I}$) assumes that the value of noise power at all electrodes is one (or the variance of all electrodes is one). It is obvious that this structure is an unsuitable structure and is not realistic because it does not use any information about the measurements under study. In this study, we applied five different structures to improve the estimation of the covariance matrix. Table 1 briefly presents different alternative structures proposed for $\mathbf{R_0}$. The first and second structures are extended versions of the $\mathbf{R_0} = \mathbf{I}$. These structures consider uniform noise power for all electrodes. According to Table 1, in the first and second structures, the value of noise power is considered equal to the average and standard deviation of the variance of the electrodes, respectively. Also, structures 4 and 5 use the same consideration i.e., the value of noise power is considered equal to the average and standard deviation of the diagonal elements of matrix, respectively. In practice, it is known that background activity is not evenly distributed on the surface of the scalp. Consequently, the power of the electrodes may be different [27,28]. With this in mind, as well as to provide a more realistic estimate, the third structure is proposed. In this structure, for each electrode, the noise power is equal to the variance of that electrode. Consequently, in this study, more realistic structures are proposed to obtain more efficient shrinkage-based estimators. Finally, Table 2 summarizes the proposed robust data covariance matrix estimators for each of the beamformer-based techniques. According to this table, a unique estimator is considered for each method.

Table 1
Alternative structures considered in this study.

Number	Proposed alternative structures
1	$\mathbf{R}_{01} = \frac{\sum(diag(\hat{\mathbf{R}}))}{N} \times \mathbf{I} = \frac{trace(\hat{\mathbf{R}})}{N} \times \mathbf{I}$
2	$\mathbf{R}_{02} = std(diag(\hat{\mathbf{R}})) \times \mathbf{I}$
3	$\mathbf{R}_{03} = diag(diag(\hat{\mathbf{R}}))$
4	$\mathbf{R}_{04} = \frac{\sum(diag(\hat{\mathbf{R}}^{-1}))}{N} \times \mathbf{I} = \frac{trace(\hat{\mathbf{R}}^{-1})}{N} \times \mathbf{I}$
5	$\mathbf{R}_{05} = std(diag(\hat{\mathbf{R}}^{-1})) \times \mathbf{I}$

Algorithm 2 The GLC shrinkage covariance matrix estimator.

Input: $\mathbf{S} \in \mathbb{R}^{m\times n\times r}$: The total number of segments extracted from the training dataset.

Output: $\tilde{\mathbf{R}}^j_{GLC}$ and $\mathbf{w}^i_{GLC}$, where $i \in [1,\ldots,32]$ and $j \in [1,\ldots,5]$ are the number of selectable targets and proposed structure, respectively.

1: Extracted all the segments for target i : $\mathbf{S_i} \in \mathbb{R}^{m\times n\times k}$

2: $\mathbf{A_i} \in \mathbb{R}^{m\times n} = \frac{1}{k}\sum_{j=1}^{k}\mathbf{S}_i(m,n,j)$,

3: Calculate $\mathbf{a}_i^T \in \mathbb{R}^{1\times(mn)} = concat\,(\mathbf{A_i} \in \mathbb{R}^{m\times n})$

4: Concatenate rows of the segments, i.e., $\mathbf{E} \in \mathbb{R}^{(mn)\times r} = concat\,(\mathbf{S} \in \mathbb{R}^{m\times n\times r})$,

5: Remove the mean of $\mathbf{E}$: $\mathbf{E} = \mathbf{E} - mean(\mathbf{E})$

6: Calculate the sample covariance matrix $\hat{\mathbf{R}} \in \mathbb{R}^{(mn)\times(mn)} = \frac{1}{r-1}\mathbf{E}\mathbf{E}^T$,

7: Use one of the proposed structures from the Table 1 to calculate $\mathbf{R}_{0j}$ where $j \in [1,\ldots,5]$,

8: Compute $\hat{\rho}$, $\hat{\nu}$, and $\hat{\gamma}$ using Equations 9, 10, and 11, respectively.

9: Calculate the values of $\hat{\beta}_{0j}$ and $\hat{\alpha}_{0j}$ using the equations 13 and 14, respectively

10: Calculate $\tilde{\mathbf{R}}_{\mathbf{GLC_j}} = \hat{\alpha}_{0j}\mathbf{R}_{0j} + \hat{\beta}_{0j}\hat{\mathbf{R}}$,

11: Use the Lagrange multipliers to build the GLC-based beamformer as follows:

$\mathbf{w}_{GLC_i} = \frac{(\tilde{\mathbf{R}}_{\mathbf{GLC}})^{-1}\mathbf{a}_i}{\mathbf{a}_i^T(\tilde{\mathbf{R}}_{\mathbf{GLC}})^{-1}\mathbf{a}_i}$

12: **return** 32 beamformers (each for one target)

Table 2
Alternative robust covariance matrix estimators.

n	ID	Proposed alternative covariance matrix
1	STB	$\tilde{\mathbf{R}}_{\mathbf{STB}} = \hat{\mathbf{R}}$
2	DL	$\tilde{\mathbf{R}}_{DL} = (0.05 \times \mathbf{R}_0) + (0.95 \times \hat{\mathbf{R}})$
3	CC_1	$\tilde{\mathbf{R}}_{\mathbf{CC_1}} = \hat{\lambda}_{01}\mathbf{R}_{01} + (1 - \hat{\lambda}_{01})\hat{\mathbf{R}}$
4	CC_2	$\tilde{\mathbf{R}}_{\mathbf{CC_2}} = \hat{\lambda}_{02}\mathbf{R}_{02} + (1 - \hat{\lambda}_{02})\hat{\mathbf{R}}$
5	CC_3	$\tilde{\mathbf{R}}_{\mathbf{CC_3}} = \hat{\lambda}_{03}\mathbf{R}_{03} + (1 - \hat{\lambda}_{03})\hat{\mathbf{R}}$
6	CC_4	$\tilde{\mathbf{R}}_{\mathbf{CC_4}} = \hat{\lambda}_{04}\mathbf{R}_{04} + (1 - \hat{\lambda}_{04})\hat{\mathbf{R}}$
7	CC_5	$\tilde{\mathbf{R}}_{\mathbf{CC_5}} = \hat{\lambda}_{05}\mathbf{R}_{05} + (1 - \hat{\lambda}_{05})\hat{\mathbf{R}}$
8	GLC_1	$\tilde{\mathbf{R}}_{\mathbf{GLC_1}} = \hat{\alpha}_{01}\mathbf{R}_{01} + \hat{\beta}_{01}\hat{\mathbf{R}}$
9	GLC_2	$\tilde{\mathbf{R}}_{\mathbf{GLC_2}} = \hat{\alpha}_{02}\mathbf{R}_{02} + \hat{\beta}_{02}\hat{\mathbf{R}}$
10	GLC_3	$\tilde{\mathbf{R}}_{\mathbf{GLC_3}} = \hat{\alpha}_{03}\mathbf{R}_{03} + \hat{\beta}_{03}\hat{\mathbf{R}}$
11	GLC_4	$\tilde{\mathbf{R}}_{\mathbf{GLC_4}} = \hat{\alpha}_{04}\mathbf{R}_{04} + \hat{\beta}_{04}\hat{\mathbf{R}}$
12	GLC_5	$\tilde{\mathbf{R}}_{\mathbf{GLC_5}} = \hat{\alpha}_{05}\mathbf{R}_{05} + \hat{\beta}_{05}\hat{\mathbf{R}}$

In the above structures, $\hat{\lambda}_{0i}$ is calculated using the CC_i method, where $i \in [1, \ldots, 5]$. Also, $\hat{\alpha}_{0i}$ and $\hat{\beta}_{0i}$ are calculated using the GLC_i technique.

2.5. Classification

As shown in Fig. 1, the classification step consists of two processes, i.e., thresholding and maximization. For each target, the four-fold cross-validation technique and the receiver operating characteristic (ROC) curve criterion were used to determine the optimal threshold value. Since the maximum value of the classification accuracy is likely to be obtained for different threshold values, the median of the obtained thresholds is considered as the optimal threshold value. In order to classify a new epoch, as shown in Fig. 1, the segments are first extracted from the input epoch. Then, the two processes of averaging and concatenation are performed on the extracted segments. The resulting vector is filtered using all the beamformers designed in the training step to obtain the beamformers' output vector (i.e., $\mathbf{y} = y_1, y_2, \ldots, y_{32}$). Afterward, a new vector (i.e., $\mathbf{c} = c_1, c_2, \ldots, c_{32}$) is obtained by applying the thresholding process to the vector $\mathbf{y}$. Among the obtained values, the scores greater than their corresponding threshold (i.e., $\{c_i | c_i > th_i\}, \quad i = 1, 2, \ldots, 32$) are selected. Among the selected values, the score with the highest value is considered as a winner, and it determines the label of the input epoch. If none of the output values of $\mathbf{c}$ are greater than their corresponding threshold, the largest value of $\mathbf{c}$ is selected as the winner. We also compare the performance of the proposed spatiotemporal beamformer-based techniques with the three classification models including SVM, K-nearest neighbor (KNN), and linear discriminant analysis (LDA) [29]. The key steps for implementing the SVM, KNN, and LDA classifiers are shown in Fig. 2. As illustrated in Fig. 2, in both the training and testing phases, the beamformers' output (i.e., $\mathbf{y} = y_1, y_2, \ldots, y_{32}$) was considered as a feature vector and fed into the mentioned classifiers. It should be noted that the SVM, KNN, and LDA classifiers have been implemented using the *fitcecoc*, *fitcknn*, and *fitcdiscr* MATLAB functions, respectively.

2.6. Metrics for performance evaluating

In practice, various criteria are used to evaluate the performance of BCI systems. The information transfer rate (ITR) is the standard method, and it is the most important metric for measuring the performance of BCI systems. ITR can be defined in bits/minute as follows:

$$ITR = \left(\log_2(M) + P\log_2(P) + (1-P)\log_2\left[\frac{1-P}{M-1}\right]\right) \times \left(\frac{60}{T}\right) \tag{19}$$

where M, P, and T represent the number of targets, classification accuracy, and the time is needed for target selection, respectively.

3. Results

The performance of beamforming-based methods is highly dependent on the estimation of the covariance matrix. When a smaller sample size is available (i.e., a shorter stimulation time), the performance of conventional methods decreases. In order to improve the performance of the conventional STB method, this study proposes 10 different structures to improve the estimation of the covariance matrix (Table 2). In the current study, the five-fold cross-validation technique was used to evaluate the perfor-

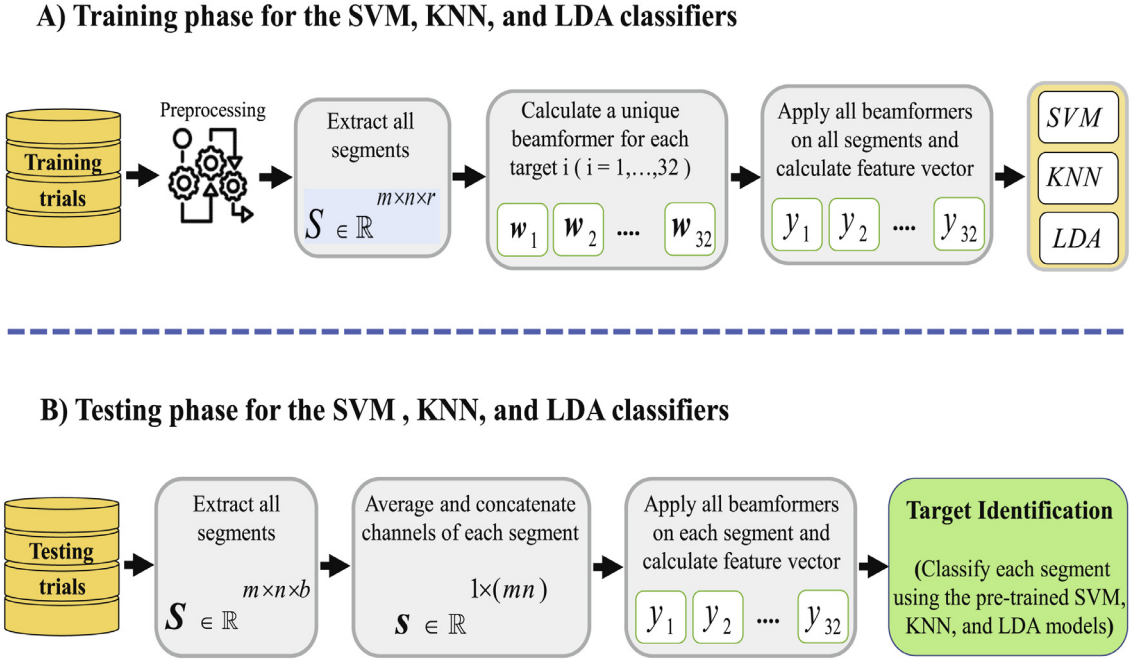

Fig. 2. The key steps for implementing the SVM, KNN, and LDA classifiers in (A) training and (B) testing phases.

Table 3
For accuracy metric, the mean and standard deviation values of STB, DL, CC_1, CC_2, CC_3, CC_4, CC_5, GLC_1, GLC_2, GLC_3, GLC_4, and GLC_5 are listed. At each stimulation time, the average of classification accuracies of 17 subjects is reported.

Method	Criteria	Stimulation time (second)									
		0.525	1.05	1.575	2.1	2.625	3.150	3.675	4.20	4.725	5.250
STB	mean	41.54	73.20	86.18	91.99	93.93	95.59	96.91	97.39	98.16	98.31
	std	15.51	19.43	15.78	11.90	10.27	8.46	6.43	6.06	4.25	4.02
DL	mean	63.24	88.57	94.30	97.17	98.16	98.71	99.19	99.26	99.19	99.42
	std	14.30	9.93	7.92	5.35	3.88	2.67	1.90	1.90	2.17	1.60
CC_1	mean	65.11	89.37	95.33	97.50	98.57	99.04	99.38	99.67	99.74	99.74
	std	13.53	10.07	6.39	5.16	3.27	2.51	1.51	1.06	0.77	0.67
CC_2	mean	64.52	89.01	94.71	97.65	98.31	98.97	99.34	99.49	99.67	99.74
	std	13.89	10.43	6.88	4.81	3.55	2.51	1.63	1.40	0.94	0.67
CC_3	mean	65.07	89.49	95.37	97.72	98.71	99.26	99.49	99.60	99.78	99.78
	std	13.45	10.01	6.40	4.72	3.18	1.98	1.38	1.23	0.62	0.62
CC_4	mean	64.60	88.86	94.85	97.68	98.24	98.97	99.30	99.49	99.60	99.78
	std	13.95	10.23	7.61	4.81	3.70	2.47	1.70	1.40	1.36	0.62
CC_5	mean	64.36	88.82	94.71	97.57	98.27	98.93	99.38	99.49	99.52	99.74
	std	14.17	10.16	7.74	4.96	3.69	2.61	1.50	1.40	1.52	0.77
GLC_1	mean	65.00	89.30	95.37	97.54	98.57	99.08	99.41	99.63	99.74	99.74
	std	13.52	10.15	6.40	5.18	3.27	2.37	1.46	1.08	0.77	0.67
GLC_2	mean	65.00	89.30	95.37	97.54	98.57	99.08	99.41	99.63	99.74	99.74
	std	13.52	10.15	6.40	5.18	3.27	2.37	1.46	1.08	0.77	0.67
GLC_3	mean	64.93	89.45	95.55	97.76	98.82	99.26	99.41	99.63	99.74	99.78
	std	12.93	10.40	6.08	4.68	3.08	1.87	1.55	1.08	0.67	0.54
GLC_4	mean	65.0	89.30	95.37	97.54	98.57	99.08	99.41	99.63	99.74	99.74
	std	13.52	10.15	6.40	5.18	3.27	2.37	1.46	1.08	0.77	0.67
GLC_5	mean	65.0	89.30	95.37	97.54	98.57	99.08	99.41	99.63	99.74	99.74
	std	13.52	10.15	6.40	5.18	3.27	2.37	1.46	1.08	0.77	0.67

mance of the implemented methods. Moreover, two criteria, i.e., ITR (bits/min) and classification accuracy, were used to measure and compare the performance of different methods. The results of previous studies show that STB-based techniques perform better than the CCA method in both m-sequence and chaotic codes [2]. Therefore, in this work, the performance of all the proposed approaches was compared with that of the STB technique. The mean and standard deviation of the classification accuracy for all the proposed methods over the stimulation time are reported in Table 3. According to this table, for the shortest stimulation time (i.e., 0.525 seconds), the highest average classification accuracy of 65.11% is obtained using the proposed CC_1 method. It is noteworthy that there is no significant difference between the results of the proposed methods. However, all the proposed methods perform better than the conventional STB method in terms of classification accuracy. According to Table 3, our proposed methods improved the classification accuracy by an average of 20% compared to the conventional STB method for the 0.525 second stimulation time. It is worth mentioning that increasing the stimulation time results in a better estimate of the covariance matrix, thus improving the performance of all the methods. In addition, the performance of the GLC_3, CC_3, DL, and STB methods was compared in terms of the classification accuracy in Fig. 3. As indicated in this figure, all three proposed techniques perform better than the STB method.

The mean and standard deviation of the ITR criterion obtained for different methods are summarized in Table 4. For each stimulation time, the mean of ITRs of 17 subjects was calculated and reported. As reported in this table, it is clear that all the proposed methods perform better than the conventional STB technique over all the stimulation times. The highest and lowest averages of ITR for the stimulation time of 1.05 seconds were obtained using the GLC_3 (an average ITR of 157.07 bits/min) and STB (an average ITR of 114.82 bits/min) methods, respectively. Moreover, Fig. 4 compares the performance of the proposed methods with that of the STB technique in terms of ITR. According to this figure, for all stimulation times, the proposed methods perform better than the STB technique.

3.1. Statistical analysis

The Wilcoxon rank-sum test is usually used to determine whether two dependent samples have been selected from populations with the same distribution. In this study, we used the Wilcoxon rank-sum test to compare the accuracies of the GLC_3 and CC_3 methods with that of the STB technique for different stimulation times. The Z-values and P-values are reported in Table 5. According to this table, for the shortest stimulation time, there are significant differences between the performance of our proposed methods, i.e., GLC_3 (P-value$= 1.62 \times 10^{-4}$) and CC_3 (P-value$= 1.99 \times 10^{-4}$) techniques, and that of the conventional STB method. When the stimulation time is increased, more samples become available. Consequently, more accurate estimations of the covariance matrix can be obtained, and the performance of all the implemented methods will improve. As a result, the Wilcoxon rank-sum test showed no significant changes when the accuracies of the proposed methods and the STB technique were compared for the long stimulation times (Z-value $=$ 1.58, P-value $=$ 0.11330). However, for all the stimulation times, the proposed methods outperform the STB method.

3.2. Training time

Fig. 5 compares the training times of three classifiers, including the STB, GLC_3, and SVM methods for the stimulus presentation frequency of 120 *Hz*. According to this figure, both STB and GLC methods are significantly faster than the SVM classifier. With an average training time of 5.05 seconds, the STB technique yields the shortest training time followed by the proposed GLC_3 method with 5.78 seconds. Whereas the SVM classifier requires the longest training time (with an average training time of 32.14 seconds).

4. Discussion

In this study, a novel framework for identifying cVEP responses was developed using adaptive shrinkage-based covariance matrix

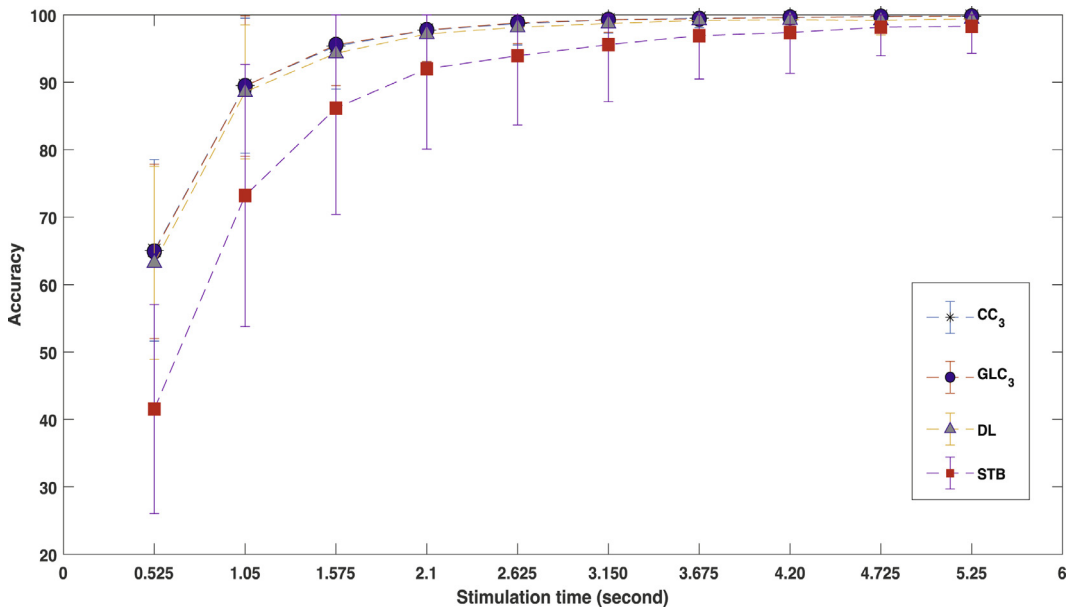

Fig. 3. Target detection accuracies provided using the five-fold cross-validation with STB, DL, GLC_3, and CC_3 techniques over stimulation time. It is clear that with increasing stimulation time, the classification accuracy increases in all the methods.

Table 4
For ITR metric, the mean and standard deviation values of STB, DL, CC_1, CC_2, CC_3, CC_4, CC_5, GLC_1, GLC_2, GLC_3, GLC_4, and GLC_5 are listed. At each stimulation time, the average of ITR (bits/min) of 17 subjects is reported.

Method	Criteria	Stimulation time (second)									
		0.525	1.05	1.575	2.1	2.625	3.150	3.675	4.20	4.725	5.250
STB	mean	69.98	114.82	111.63	99.19	85.60	75.56	67.65	60.69	55.31	50.40
	std	40.32	45.74	30.81	19.94	14.84	11.02	7.72	6.53	4.39	3.80
DL	mean	134.05	154.04	128.99	108.95	92.41	79.93	70.58	62.81	56.44	51.50
	std	46.03	28.22	17.94	10.71	6.87	4.35	2.8399	2.53	2.54	1.77
CC_1	mean	140.09	156.70	131.43	109.69	93.13	80.53	70.85	63.34	57.06	51.84
	std	44.60	28.83	15.41	10.33	5.90	4.05	2.34	1.49	1.01	0.83
CC_2	mean	138.24	155.67	129.81	109.98	92.63	80.39	70.79	63.08	56.97	51.84
	std	45.56	29.64	16.23	9.77	6.32	4.05	2.47	1.91	1.22	0.83
CC_3	mean	139.92	156.99	131.52	110.10	93.42	80.87	71.01	63.24	57.10	51.89
	std	44.19	28.48	15.34	9.53	5.69	3.28	2.12	1.69	0.85	0.77
CC_4	mean	138.53	155.08	130.37	110.06	92.51	80.37	70.74	63.08	56.90	51.89
	std	46.01	28.89	17.34	9.75	6.54	3.99	2.57	1.91	1.65	0.77
CC_5	mean	137.75	154.97	130.031	109.84	92.58	80.33	70.84	63.08	56.81	51.85
	std	46.34	28.92	17.60	10.02	6.52	4.17	2.31	1.91	1.83	0.92
GLC_1	mean	139.70	156.48	131.53	109.79	93.13	80.58	70.90	63.27	57.06	51.84
	std	44.44	28.94	15.42	10.36	5.90	3.87	2.25	1.53	1.01	0.83
GLC_2	mean	139.70	156.48	131.53	109.79	93.13	80.58	70.90	63.27	57.06	51.84
	std	44.44	28.94	15.42	10.36	5.90	3.87	2.25	1.53	1.01	0.83
GLC_3	mean	139.17	157.07	131.98	110.19	93.68	80.86	70.91	63.29	57.05	51.88
	std	42.51	29.58	14.86	9.45	5.60	3.14	2.35	1.53	0.91	0.69
GLC_4	mean	139.70	156.48	131.53	109.79	93.13	80.58	70.90	63.29	57.06	51.84
	std	44.44	28.94	15.42	10.36	5.89	3.87	2.25	1.53	1.01	0.83
GLC_5	mean	139.70	156.48	131.53	109.79	93.13	80.58	70.90	63.27	57.06	51.84
	std	44.44	28.94	15.42	10.36	5.89	3.87	2.25	1.53	1.01	0.83

estimators and beamformer-based techniques. As mentioned in previous sections, the performance of beamformer-based methods is highly dependent on the estimation of the data covariance matrix. As the stimulation time decreases, the number of available time samples decreases as well. Therefore, an accurate and robust estimate of the covariance matrix cannot be obtained. As a result, the performance of conventional methods is severely reduced for short stimulation times. Therefore, in order to provide a robust and reliable estimate of the covariance matrix, various structures are proposed in this study (Table 2).

The classification accuracies of the proposed methods and the STB technique are reported in Table 3. As presented in this table, for all stimulation times, all the proposed methods provided a higher classification accuracy than the STB approach. According to this table, the results of the DL method are comparable to those of the GLC and CC-based techniques. However, the determination of the proper DL factor has always been a challenging issue that needs expert knowledge. In this study, the optimal value of the DL factor for each subject was individually obtained using a greedy search algorithm. As mentioned in previous sections, in all the proposed GLC and CC-based approaches, all the parameters are automatically and adaptively determined using the MSE concept.

As reported in Table 3, for the shortest stimulation time, the highest classification performances were provided using the CC_1

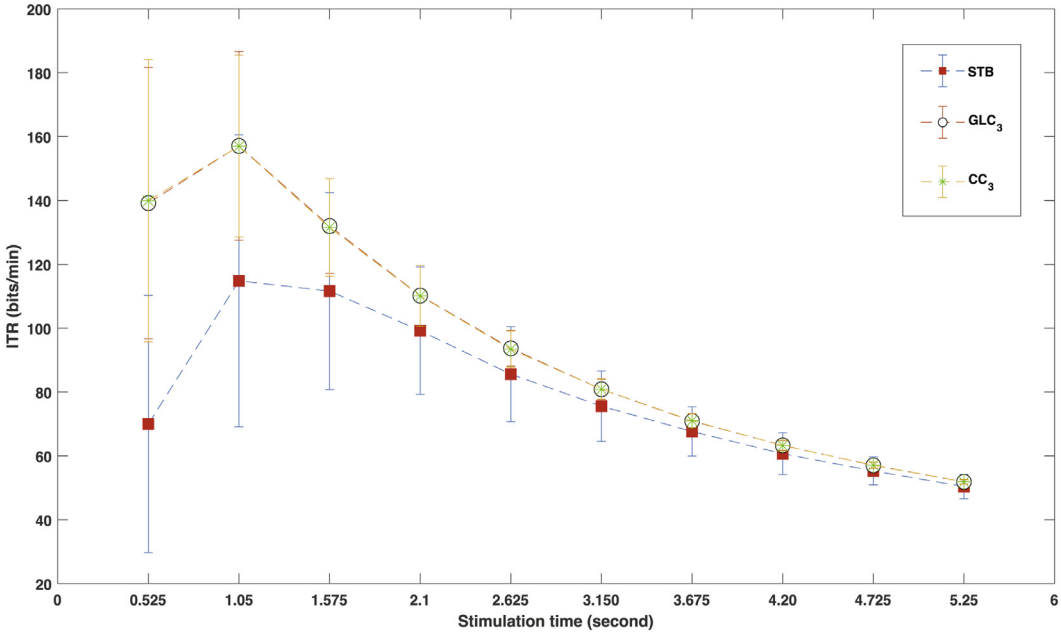

Fig. 4. The ITR values of STB, GLC_3, and CC_3 techniques. These results were obtained by considering 0.5 seconds for the subject's gaze-switching time.

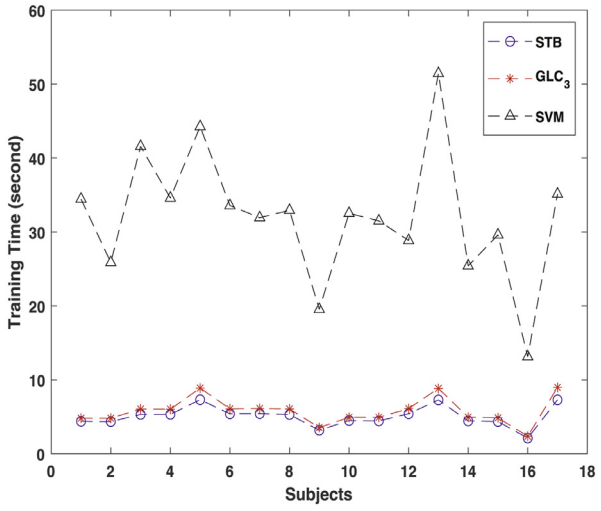

Fig. 5. The required training times to train different classifiers on all epochs of each subject. The stimulus presentation frequency and stimulation time of 120 Hz and 1.05 seconds are considered, respectively.

Table 5
The results of statistical comparison of the GLC_3 and CC_3 accuracy rates with those of STB method through Wilcoxon rank-sum test.

Stimulation time	GLC_3 vs STB		CC_3 vs STB	
(second)	Z-value	P-value	Z-value	P-value
0.525	3.77	1.62×10^{-4}	3.72	1.99×10^{-4}
1.05	3.02	0.00256	3.03	0.00241
1.575	2.35	0.01892	2.29	0.02175
2.1	2.49	0.01274	2.52	0.01166
2.625	2.73	0.00631	2.43	0.01503
3.150	2.45	0.01414	2.49	0.01275
3.675	2.05	0.04058	2.09	0.03683
4.20	1.58	0.11342	1.58	0.11342
4.725	1.79	0.07397	1.87	0.06107
5.250	1.58	0.11330	1.61	0.10830

(the average accuracy of 65.11%) and CC_3 (the average accuracy of 65.07%) methods, respectively. However, there is no significant difference between the proposed methods in terms of performance. For a more clear presentation, the performance of the GLC_3, CC_3, DL and STB methods was compared in terms of classification accuracy in Fig. 3. According to this figure, all three proposed methods outperform the conventional STB technique over all the stimulation times. Moreover, for the shortest stimulation time, all our proposed methods have improved the average classification accuracy by at least 20%. Finally, the results show that the proposed methods improve the classification accuracy for all stimulation times. As shown in Fig. 3, as the stimulation time increases, a better estimate of the covariance matrix is provided, resulting in the improved performance of all the methods. However, increasing the stimulation time reduces the value of ITR (Table 4) and causes mental fatigue.

In Table 4, the results of comparing the performance of the proposed methods and the STB technique in terms of ITR are presented. According to this table, all the proposed methods outperform the conventional STB technique over all the stimulation times. In other words, the highest and lowest ITR values were obtained using the GLC_3 and STB methods, respectively. It is noteworthy that the maximal average ITR value of 157.07 bits/min was obtained at the stimulation time of 1.05 seconds using the GLC_3 method.

In addition, Fig. 4 compares the performance of the STB, CC_3, and GLC_3 methods in terms of ITR. According to this figure, both of the proposed CC_3 and GLC_3 methods perform better than the STB technique over all stimulation times.

Furthermore, Fig. 6 compares the performance of the proposed GLC_3 and CC_3 methods with that of other conventional classifiers, such as SVM, KNN, and LDA. As can be seen from this figure, our proposed methods (i.e., CC_3 and GLC_3) perform better than the conventional classifiers, including SVM, KNN, and LDA over all stimulation times. Moreover, as indicated in Fig. 5, the beamformer-based techniques require only a fraction of time required to train the SVM classifier. It should be noted that in addition to the proposed methods, there are other adaptive approaches that can be used to improve the estimation of the covariance matrix and thus

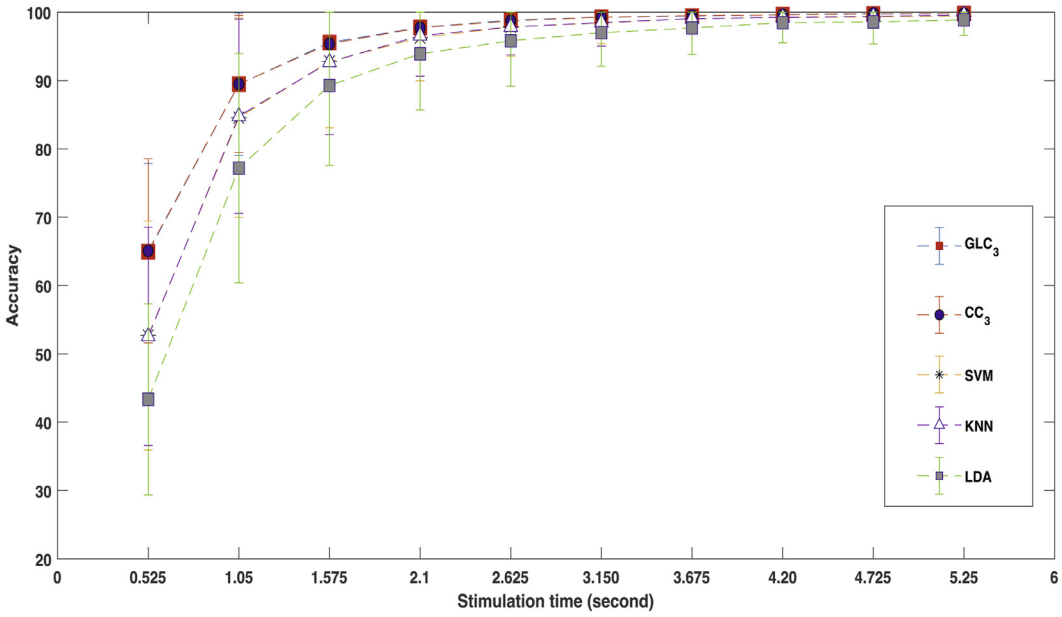

Fig. 6. Target detection accuracies of the STB, DL, GLC_3, and CC_3 techniques over stimulation time. The performance of all methods improves in terms of classification accuracy with increasing stimulation time.

improve the performance of the cVEP-based BCI systems [30,31]. In our future works, we will investigate the performance of the adaptive detectors for cVEP target identification.

5. Conclusion

For the first time, this study examined the effectiveness of shrinkage-based adaptive covariance matrix estimators in the application of cVEP-based BCI systems. All the proposed methods automatically provide more robust covariance matrix estimations over short stimulation times, thus improving the performance of conventional STB-based techniques. The results show that our proposed approaches outperform the conventional STB method as they improve the average classification accuracy by at least 20%. Moreover, we have shown that all the proposed methods can compete with some of the optimized classifiers, such as SVM, KNN, and LDA models. The results show that using two repetitions of the stimulation time is sufficient for obtaining the maximal average ITR value of 157.07 bits/min. We suggest the use of knowledge-aided adaptive covariance matrix estimators for improving the performance of the conventional c-VEP-based BCI systems and developing more robust algorithms.

Declaration of Competing Interest

The authors declare that they have no known competing financial interests or personal relationships that could have appeared to influence the work reported in this paper.

References

[1] G. Bin, X. Gao, Y. Wang, B. Hong, S. Gao, VEP-based brain-computer interfaces: time, frequency, and code modulations [research frontier], IEEE Comput Intell Mag 4 (4) (2009) 22–26.
[2] Z. Shirzhiyan, A. Keihani, M. Farahi, E. Shamsi, M. GolMohammadi, A. Mahnam, M.R. Haidari, A.H. Jafari, Introducing chaotic codes for the modulation of code modulated visual evoked potentials (c-VEP) in normal adults for visual fatigue reduction, PLoS ONE 14 (3) (2019) e0213197.
[3] M.N. Yasinzai, Y.Z. Ider, New approach for designing cVEP BCI stimuli based on superposition of edge responses, Biomedical Physics & Engineering Express 6 (4) (2020) 045018.
[4] D.-O. Won, H.-J. Hwang, S. Dähne, K.-R. Müller, S.-W. Lee, Effect of higher frequency on the classification of steady-state visual evoked potentials, J Neural Eng 13 (1) (2015) 016014.
[5] D. Aminaka, S. Makino, T.M. Rutkowski, Chromatic and high-frequency cVEp-based BCI paradigm, in: 2015 37th Annual International Conference of the IEEE Engineering in Medicine and Biology Society (EMBC), IEEE, 2015, pp. 1906–1909.
[6] T. Başaklar, Y. Tuncel, Y.Z. Ider, Effects of high stimulus presentation rate on EEG template characteristics and performance of c-VEP based BCIs, Biomedical Physics & Engineering Express 5 (3) (2019) 035023.
[7] D. Aminaka, S. Makino, T.M. Rutkowski, Classification accuracy improvement of chromatic and high-frequency code-modulated visual evoked potential–based BCI, in: International Conference on Brain Informatics and Health, Springer, 2015, pp. 232–241.
[8] Q. Wei, Y. Liu, X. Gao, Y. Wang, C. Yang, Z. Lu, H. Gong, A novel c-VEP BCI paradigm for increasing the number of stimulus targets based on grouping modulation with different codes, IEEE Trans. Neural Syst. Rehabil. Eng. 26 (6) (2018) 1178–1187.
[9] J. Thielen, P. Marsman, J. Farquhar, P. Desain, From full calibration to zero training for a code-modulated visual evoked potentials for brain–computer interface, J Neural Eng 18 (5) (2021) 056007.
[10] F. Roque, G. Pires, J. Perdiz, U.J. Nunes, A user identification system based on code-modulated visual evoked potentials with LED stimulation, in: 2021 IEEE International Workshop on Biometrics and Forensics (IWBF), IEEE, 2021, pp. 1–6.
[11] B. Wittevrongel, E. Van Wolputte, M.M. Van Hulle, Code-modulated visual evoked potentials using fast stimulus presentation and spatiotemporal beamformer decoding, Sci Rep 7 (1) (2017) 1–10.
[12] Y. Jiang, Y. Kang, P. Wang, S. Ge, Filter bank spatiotemporal beamforming for frequency detection in SSVEP-based BCI, in: 2019 IEEE EMBS International Conference on Biomedical & Health Informatics (BHI), IEEE, 2019, pp. 1–4.
[13] M. Van Vliet, N. Chumerin, S. De Deyne, J.R. Wiersema, W. Fias, G. Storms, M.M. Van Hulle, Single-trial erp component analysis using a spatiotemporal LCMV beamformer, IEEE Trans. Biomed. Eng. 63 (1) (2015) 55–66.
[14] S. Ge, Y. Jiang, P. Wang, H. Wang, W. Zheng, Training-free steady-state visual evoked potential brain–computer interface based on filter bank canonical correlation analysis and spatiotemporal beamforming decoding, IEEE Trans. Neural Syst. Rehabil. Eng. 27 (9) (2019) 1714–1723.
[15] D. Gutiérrez, D.I. Escalona-Vargas, EEG data classification through signal spatial redistribution and optimized linear discriminants, Comput Methods Programs Biomed 97 (1) (2010) 39–47.
[16] D. Cheyne, L. Bakhtazad, W. Gaetz, Spatiotemporal mapping of cortical activity accompanying voluntary movements using an event-related beamforming approach, Hum Brain Mapp 27 (3) (2006) 213–229.
[17] B. Wittevrongel, M.M. Van Hulle, Faster P300 classifier training using spatiotemporal beamforming, Int J Neural Syst 26 (03) (2016) 1650014.
[18] M. Sabeti, S. Katebi, K. Rastgar, Z. Azimifar, A multi-resolution approach to localize neural sources of P300 event-related brain potential, Comput Methods Programs Biomed 133 (2016) 155–168.

[19] S.A. Vorobyov, A.B. Gershman, Z.-Q. Luo, Robust adaptive beamforming using worst-case performance optimization: a solution to the signal mismatch problem, IEEE Trans. Signal Process. 51 (2) (2003) 313–324.
[20] M. Ravan, J.P. Reilly, G. Hasey, Minimum variance brain source localization for short data sequences, IEEE Trans. Biomed. Eng. 61 (2) (2013) 535–546.
[21] L. Du, T. Yardibi, J. Li, P. Stoica, Review of user parameter-free robust adaptive beamforming algorithms, Digit Signal Process 19 (4) (2009) 567–582.
[22] X. Gou, Z. Liu, J. Ma, Y. Xu, User-parameter-free robust adaptive beamforming algorithm for vector-sensor arrayswithin the hypercomplex framework, Journal of Electrical Engineering 64 (2) (2013) 100.
[23] B. Wittevrongel, M.M. Van Hulle, Spatiotemporal beamforming: a transparent and unified decoding approach to synchronous visual brain-computer interfacing, Front Neurosci 11 (2017) 630.
[24] L. Beltrachini, N. von Ellenrieder, C.H. Muravchik, Shrinkage approach for spatiotemporal EEG covariance matrix estimation, IEEE Trans. Signal Process. 61 (7) (2013) 1797–1808.
[25] A.T. Jafadideh, B.M. Asl, Modified dominant mode rejection beamformer for localizing brain activities when data covariance matrix is rank deficient, IEEE Trans. Biomed. Eng. 66 (8) (2018) 2241–2252.
[26] A.Y. Kaplan, S.L. Shishkin, I.P. Ganin, I.A. Basyul, A.Y. Zhigalov, Adapting the p300-based brain–computer interface for gaming: a review, IEEE Trans. Comput. Intell. AI Games 5 (2) (2013) 141–149.
[27] Z. Liu, M. Fukunaga, J.A. de Zwart, J.H. Duyn, Large-scale spontaneous fluctuations and correlations in brain electrical activity observed with magnetoencephalography, Neuroimage 51 (1) (2010) 102–111.
[28] A.d. De Jongh, J. De Munck, J. Baayen, E. Jonkman, R. Heethaar, B. Van Dijk, The localization of spontaneous brain activity: first results in patients with cerebral tumors, Clinical Neurophysiology 112 (2) (2001) 378–385.
[29] R.O. Duda, P.E. Hart, et al., Pattern classification, John Wiley & Sons, 2006.
[30] W. Liu, W. Xie, R. Li, Z. Wang, Y. Wang, Adaptive detectors in the krylov subspace, Science China Information Sciences 57 (10) (2014) 1–11.
[31] Y. Wang, W. Liu, W. Xie, Y. Zhao, Reduced-rank space-time adaptive detection for airborne radar, Science China Information Sciences 57 (8) (2014) 1–11.